



Article

The Effect of Molecular Isomerism on the Barrier Properties of Polyimides: Perspectives from Experiments and Simulations

Yiwu Liu ¹, Fengyun Xie ¹, Jie Huang ¹, Jinghua Tan ^{1,*}, Chengliang Chen ¹, Linbing Jiang ¹, Wei Sun ¹ and Hailiang Zhang ²

- ¹ National and Local Joint Engineering Center of Advanced Packaging Materials R & D Technology, Key Laboratory of Advanced Packaging Materials and Technology of Hunan Province, School of Packaging and Materials Engineering, Hunan University of Technology, Zhuzhou 412007, China; liuyiwu@hut.edu.cn (Y.L.); xie15273335456@163.com (F.X.); huangjie3@sjtu.edu.cn (J.H.); chenchengliangc@163.com (C.C.); jianglinbing123@163.com (L.J.); s2825948402@163.com (W.S.)
- ² Key Laboratory of Polymeric Materials and Application Technology of Hunan Province, Key Laboratory of Advanced Functional Polymer Materials of Colleges, Universities of Hunan Province, College of Chemistry, Xiangtan University, Xiangtan 411105, China; hailiangzhang@xtu.edu.cn
- * Correspondence: tjh@hut.edu.cn

Abstract: A novel carbazole-containing diamine (M-2,7-CPDA) isomer of our previously reported diamine 2,7-CPDA, has been synthesized using a two-step synthesis. Compared with 2,7-CPDA, the substituted position of amino is changed from *para* to *meta* for M-2,7-CPDA. The two diamines were polymerized with pyromellitic dianhydride (PMDA) to prepare two isomeric polyimides (M-2,7-CPPI and 2,7-CPPI), respectively. The effects of *para/meta* isomerism on microstructures and gas barrier performances of the two isomeric polyimides were studied by positron annihilation test, X-ray diffraction and molecular simulation. The results display that *meta*-connected M-2,7-CPPI has less ordered chain structure and weaker hydrogen bonding than *para*-connected 2,7-CPPI, which leads to loose chain stacking and thereby increased free volumes of M-2,7-CPPI. The higher free volumes promote the solubility and diffusivity of gas in M-2,7-CPPI. As a result, the *meta*-linked M-2,7-CPPI shows a lower gas barrier than its *para*-linked analog. The work provides guidance for the design and synthesis of high-performance barrier polymers.

Keywords: polyimide; isomerism; structure-property relationship; molecular simulations; barrier properties



Citation: Liu, Y.; Xie, F.; Huang, J.; Tan, J.; Chen, C.; Jiang, L.; Sun, W.; Zhang, H. The Effect of Molecular Isomerism on the Barrier Properties of Polyimides: Perspectives from Experiments and Simulations. *Polymers* **2021**, *13*, 1749. <https://doi.org/10.3390/polym13111749>

Academic Editor:
Toshihiko Matsumoto

Received: 7 March 2021
Accepted: 8 May 2021
Published: 27 May 2021

Publisher's Note: MDPI stays neutral with regard to jurisdictional claims in published maps and institutional affiliations.



Copyright: © 2021 by the authors. Licensee MDPI, Basel, Switzerland. This article is an open access article distributed under the terms and conditions of the Creative Commons Attribution (CC BY) license (<https://creativecommons.org/licenses/by/4.0/>).

1. Introduction

Barrier polymeric materials have widespread applications for the packaging of food, medicine, cosmetics, solar cells and flexible electronics display [1–3]. During usage, the barrier polymers can prevent oxygen, water vapor and other gases from penetrating into the package, thus extending the lifetime of products. Nowadays, with the rapid development of flexible electronic devices, there is an increasing demand for flexible polymer substrates with outstanding barriers as well as high heat resistance [4–6]. For instance, in the manufacturing of solar cells and active matrix organic light-emitting display devices (AMOLED), the polymer substrates are required to withstand a temperature higher than 400 °C [7–9]. At present, the most used barrier polymers include poly(ethylene terephthalate) (PET), polyethylene naphthalate (PEN), poly(vinylidene chloride) (PVDC), polyamide (PA), ethylene-vinyl alcohol copolymers (EVOH) and so on. However, these conventional barrier polymers have low thermostability and are usually used below 200 °C [10–14], which makes their application in flexible substrates difficult.

Aromatic polyimides (PIs) possess exceptional heat resistance, good mechanical and chemical performances, and have become an important material for flexible device substrates [15,16]. Most PIs exhibit a glass transition temperature (T_g) higher than 350 °C. However, conventional PIs possess poor barrier performances, which make it difficult for

them to meet the packaging requirements of electronic products [17]. Hence, the research on the barrier performances of PIs is of great significance for promoting their application in flexible substrates.

Polyimides have the advantage of structural diversity. In addition, their molecular structures possess high designability. The performances of PIs can be adjusted by structure modification. Because the substituted positions or arrangement orders are changed, PIs derived from isomeric monomers display different performances [18,19]. Many works have studied the performance of PIs derived from various isomeric diamines or dianhydrides, such as diaminodiphenyl sulfone (DDS) [20], oxydianiline (ODA) [21], bis(aminophenyl) hexafluoropropane [22], biphenyltetracarboxylic dianhydride (BPDA) [23], diphenylsulfonete-tetracarboxylic dianhydride (DSDA) [24] and diphenylthioether dianhydride (TDPA) [25]. These studies mostly focused on the influence of structural isomerism on the thermal and gas separation performances of PIs. However, no previous works have been conducted to research the isomeric effect on the barrier properties of PIs.

In our previous study, a carbazole-containing diamine monomer (2,7-CPDA, see Figure 1) was prepared and reacted with PMDA to obtain a high-barrier polyimide (2,7-CPPI) [26]. Herein, to study the isomeric effect on the barrier performances of PIs, a new diamine (M-2,7-CPDA, see Figure 1) was designed and synthesized. M-2,7-CPDA is an isomer of 2,7-CPDA, in which the substituted position of amino is changed from *para* to *meta*. The M-2,7-CPDA was then reacted with PMDA to prepare polyimide film (M-2,7-CPPI). Figure 1 shows the equilibrated conformations of repeat units for M-2,7-CPPI and 2,7-CPPI. Compared with 2,7-CPPI, M-2,7-CPPI has a larger dihedral angle between imide ring and benzene, thus leading to a more bent and distorted structure. These structural differences will affect the microstructure and thereby the barrier performances of PIs.

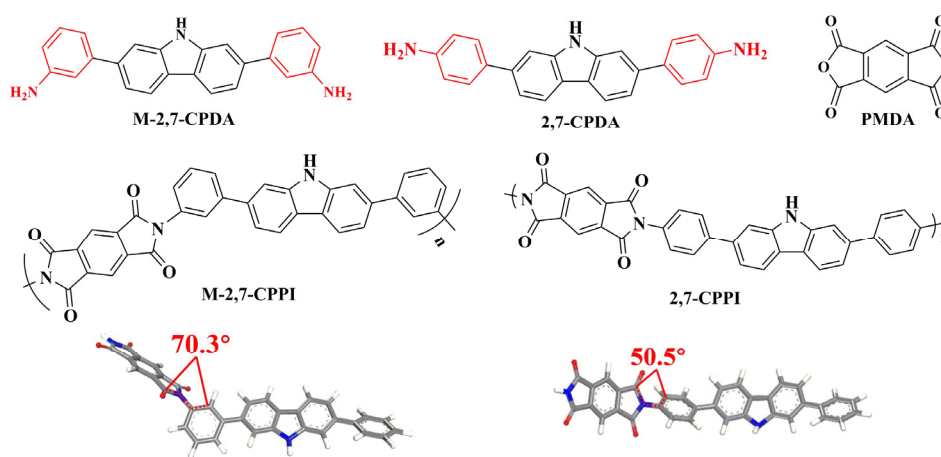


Figure 1. The chemical structures of monomers and the lowest energy conformation of M-2,7-CPPI and 2,7-CPPI repeat units.

Here, the thermal, mechanical and barrier performances of M-2,7-CPPI were investigated and compared with those of 2,7-CPPI. Molecular simulation has become an important means to study the microstructure and gas penetration of polymers at a microscale level [27]. For revealing the effect of structural isomerism on the barrier performances of PIs, molecular simulation, positron annihilation test and X-ray diffraction were adopted to analyze the chain morphology and stacking, free volume, hydrogen bonding, permeation trajectory, diffusion and adsorption behavior of PIs. This helps to understand the relationships between structures and barrier performances and provides theoretical guidance for the development of high-barrier polymers.

2. Experimental Section

2.1. Experimental Materials

Experimental materials are displayed in Supplementary Materials.

2.2. Instrumentation

Characterization instruments are shown in Supplementary Materials.

2.3. Molecular Simulation

PIs models with 5 molecular chains were constructed, where each molecular chain contains 25 repeat units. The equilibrated models were used to analyze the free volume feature, aggregation structure, gases solubility and diffusion. The model creation and simulation details are given in the Supplementary Materials.

2.4. Synthesis of 2,7-Bis(3-nitrophenyl)-9H-carbazole (M-2,7-CPDN)

3-Nitrophenylboronic acid (75 mmol), 2,7-dibromo-9H-carbazole (30 mmol) and THF (400 mL) were added in a 1000 mL three-necked flask. Then, Aliquat 336 (15 drops) and 2 M aqueous K_2CO_3 solution (112.5 mL) were placed and stirred for 0.5 h under argon at room temperature. After that, $(Pd[(C_6H_5)_3]_4)$ was added with stirring for 24 h at 75 °C. The resulting product was chromatographed on a column chromatography (dichloromethane/*n*-hexane ($v/v = 1/1$)). Yield: 85%. IR (KBr, ν , cm^{-1}): 1520 ($-NO_2$ stretching), 1262 (C–N stretching), 1086–802 (δ Ar–H). 1H NMR (400 MHz, DMSO- d_6) δ 11.54 (s, 1H), 8.54 (t, $J = 2.0$ Hz, 2H), 8.38–8.18 (m, 6H), 7.91 (d, $J = 1.2$ Hz, 2H), 7.81 (t, $J = 8.0$ Hz, 2H), 7.62 (dd, $J = 8.2, 1.6$ Hz, 2H); ^{13}C NMR (100 MHz, DMSO- d_6) δ 148.95, 143.15, 141.52, 136.19, 134.04, 130.98, 122.73, 122.30, 121.79, 118.71, 110.02; EIMS m/z (%): 409 (100) $[M]^+$, calcd for $C_{24}H_{15}N_3O_4$, 409.1, Anal. Calcd for $C_{24}H_{15}N_3O_4$: C 70.41, H 3.69, N 10.26; found: C 70.29, H 3.72, N 10.31.

2.5. Synthesis of 3,3'-(9H-Carbazole-2,7-diyl)diamino (M-2,7-CPDA)

Ethanol (450 mL) and M-2,7-CPDN (20 mmol) were poured into a three-necked flask. After heating to 80 °C, 0.5 g of 10% Pd/C catalyst and 16 mL of hydrazine monohydrate were placed into the mixture and stirred for 24 h. Then, the catalyst was cleared away by filtration. The product was collected by recrystallization. Yield: 93%. IR (KBr, ν , cm^{-1}): 3412 (N–H stretching), 1603 (δ N–H), 1262 (C–N stretching), 1086–802 (Ar–H stretching). 1H NMR (400 MHz, DMSO- d_6 , δ): 11.32 (s, 1H, NH), 8.13 (d, $J = 8.1$ Hz, 2H, Ar H), 7.64 (s, 2H, Ar H), 7.38 (dd, $J = 8.2, 1.0$ Hz, 2H, Ar H), 7.14 (t, $J = 7.8$ Hz, 2H, Ar H), 6.97 (s, 2H, Ar H), 6.89 (d, $J = 7.6$ Hz, 2H, Ar H), 6.59 (d, $J = 7.9$ Hz, 2H, Ar H), 5.18 (s, 4H, NH_2); ^{13}C NMR (100 MHz, DMSO- d_6 , δ): 149.10, 141.87, 140.80, 138.75, 129.39, 121.43, 120.36, 117.86, 114.71, 112.88, 112.48, 108.53; EIMS m/z (%): calcd for $C_{24}H_{19}N_3$, 349.16; Found: 349. $[M]^+$, Anal. Calcd for $C_{24}H_{19}N_3$: C 82.49, H 5.48, N 12.03; found: C 82.17, H 5.66, N 12.49.

2.6. Synthesis of Polyimide M-2,7-CPPI

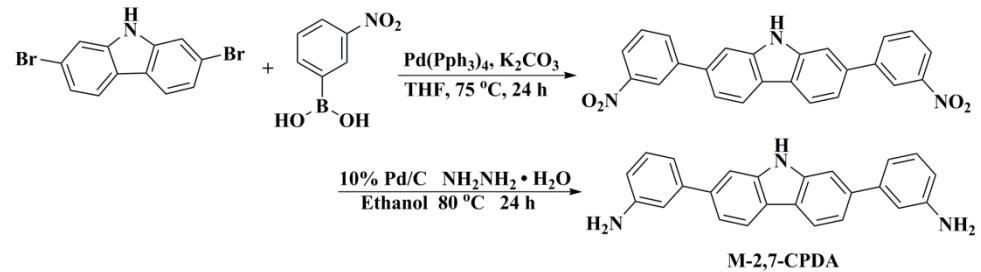
A solution of M-2,7-CPDA (12 mmol) in 18 mL of anhydrous DMF was added in a flask under argon. Then, PMDA (12 mmol) was added. After stirring for 6 h, a viscous poly(amic acid) (PAA) solution was formed. After that, the PAA precursor was casted onto a glass substrate and thermally imidized at 100 °C, 200 °C, 300 °C, and 400 °C for 1 h, respectively. The obtained polyimide membrane (M-2,7-CPPI) was then released from the substrates. IR (KBr, ν , cm^{-1}): 1776 and 1710 (imide carbonyl stretching), 1367 (imide C–N).

3. Results and Discussion

3.1. Synthesis and Characterizations of Monomers

The synthesis approach of M-2,7-CPDA is shown in Scheme 1. Firstly, M-2,7-CPDN was synthesized from 2,7-dibromo-9H-carbazole and 3-nitrophenylboronic acid by Suzuki reaction. Then, M-2,7-CPDN was reduced to diamine M-2,7-CPDA. NMR, FT-IR, elemental analyses and mass spectra were used to confirm the chemical structure of monomers. Figure S4 and Figure 2 present the NMR spectra of M-2,7-CPDN and M-2,7-CPDA, respectively. Figures S5

and S6 display the mass spectra of M-2,7-CPDN and M-2,7-CPDA, respectively. The FT-IR spectra of M-2,7-CPDN and M-2,7-CPDA are shown in Figure S7. All the above results are in accordance with the pre-designed structures of M-2,7-CPDA and M-2,7-CPDN, certifying the successful synthesis of the M-2,7-CPDA monomer.



Scheme 1. Synthesis route of M-2,7-CPDA.

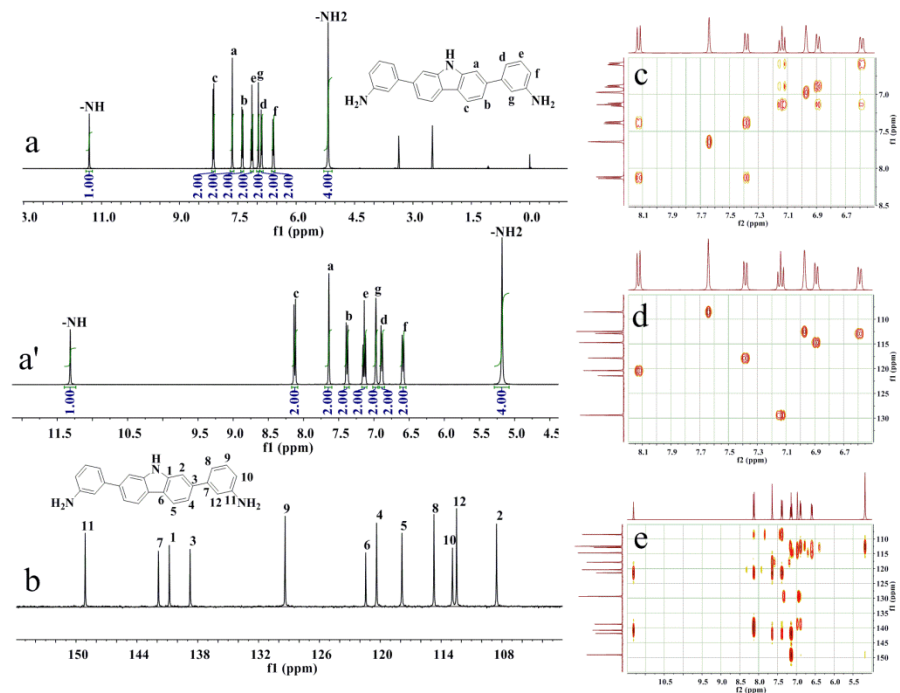
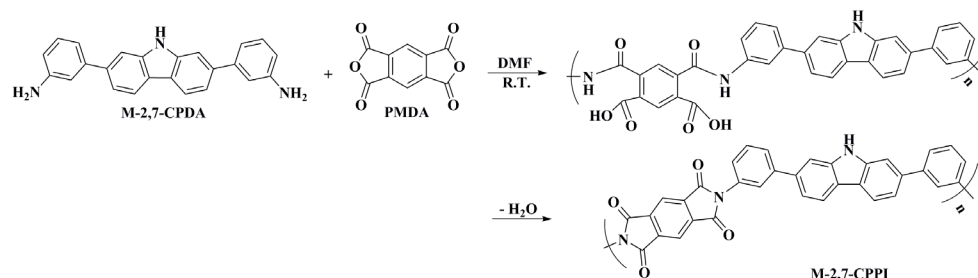


Figure 2. ^1H NMR in the range of 0~13 (a), ^1H NMR in the range of 4.5~11.5 (a'), ^{13}C NMR (b), H-H COSY (c), C-H QC (d), and C-H BC (e) spectra of M-2,7-CPDA in $\text{DMSO}-d_6$.

3.2. Synthesis and Characterizations of PI

The polyimide was formed by the two-step polycondensation reaction (Scheme 2). M-2,7-CPDA was polymerized with PMDA to prepare PAA, which was thermally cyclodehydrated to yield M-2,7-CPPI. The weight-average molecular weight (M_w) of poly(amic acid) was 6.71×10^4 and the polydispersity (PDI) was 1.95. The FT-IR spectra are displayed in Figure S7. The M-2,7-CPDA exhibited absorption bands at 3412 cm^{-1} (N–H stretching) and 1603 cm^{-1} (δ N–H), which are disappeared in M-2,7-CPPI. In addition, M-2,7-CPPI displayed absorption bands at 1776 and 1710 cm^{-1} (carbonyl stretching) and 1367 cm^{-1} (C–N stretching), indicating the successful preparation of M-2,7-CPPI membranes.



Scheme 2. Synthesis route of polyimide.

3.3. Thermal and Mechanical Performances

The thermal performances of M-2,7-CPPI are evaluated by DSC, TGA, TMA and DMA and compared with that of our previously reported *para*-isomer 2,7-CPPI. The results are shown in Figures S8–S11, and related values are summarized in Table 1. M-2,7-CPPI showed superior thermal performances with $T_{d5\%}$ and $T_{d10\%}$ of 563 °C and 601 °C (Table 1), which were comparable to that of *para*-based 2,7-CPPI. The thermostability of the two PIs was better than those of most commercial and reported aromatic PIs. This was mainly because of the planar rigid structures. From TMA and DMA curves, it can be seen that two transitions occur. The one at high temperature corresponded to glass transition (T_g), and the one at low temperature (near 120 °C) corresponded to the secondary β -relaxation [28–30]. The β -relaxation is originated from the rotational motions of local moieties [28]. Two coefficient of thermal expansion (CTE) values of M-2,7-CPPI before and after β -relaxation were determined from 40–100 °C and 150–300 °C, respectively. These are 6.39 ppm/K and 49.52 ppm/K, whereas *para*-based 2,7-CPPI exhibited a relatively low CTE of 2.89 ppm/K. The thermal expansion property of PI membranes is strongly associated with the structural linearity/rigidity of polymer chains [31]. The bent and distorted structure of M-2,7-CPPI destroyed the chain alignment, thus leading to a high CTE value. The 2,7-CPPI exhibited higher mechanical performances than M-2,7-CPPI. The linear polymer backbone structure of *para*-linked 2,7-CPPI promoted the dense chain packing and formation of hydrogen bonding, which in turn resulted in higher mechanical properties and lower CTE.

Table 1. Thermal and mechanical properties of M-2,7-CPPI and 2,7-CPPI.

| PI | T_g^1 (°C) | T_g^2 (°C) | $T_{d5\%}$ (°C) | $T_{d10\%}$ (°C) | CTE ³ (ppm·K ⁻¹) | Tensile Strength (MPa) | Tensile Modulus (GPa) | Elongation at Break (%) |
|-----------------------|-----------------|-----------------|--------------------|---------------------|--|------------------------------|-----------------------------|----------------------------|
| 2,7-CPPI ⁴ | 413 | 437 | 556 | 580 | 2.89 | 143.8 ± 3.5 | 4.5 ± 0.2 | 9.3 ± 0.4 |
| M-2,7-CPPI | 395 | 437 | 563 | 601 | 6.39, 49.52 | 120.0 ± 3.1 | 2.0 ± 0.2 | 7.6 ± 0.3 |

¹ measured by DSC; ² measured by DMA; ³ The two coefficient of thermal expansion (CTE) values of M-2,7-CPPI are determined from 40–100 °C and 150–300 °C, respectively; ⁴ The values are obtained from Ref. [26].

3.4. Barrier Properties

The gas barrier of M-2,7-CPPI is compared with 2,7-CPPI, as shown in Table 2. The *meta*-isomer M-2,7-CPPI showed favorable barrier performances with water vapor transmission rate (WVTR) and oxygen transmission rate (OTR) of 10.2 g·m⁻²·day⁻¹ and 12.1 cm³·m⁻²·day⁻¹, respectively, which are comparable to that of conventional barrier polymers such as PET and PA [32,33]. The *para*-isomer 2,7-CPPI displayed better barrier properties compared to its *meta*-counterpart M-2,7-CPPI. The barrier performance difference between the two isomeric polyimides will be discussed in the following sections from the aspects of aggregation structure, free volume, gas diffusion and solubility.

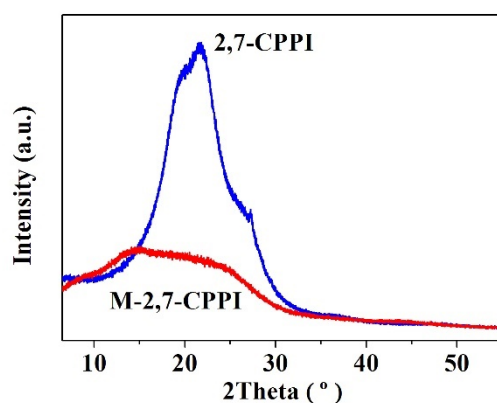
Table 2. Barrier properties M-2,7-CPPI and 2,7-CPPI films.

| PIs | WVP ($\text{g}\cdot\text{mil}\cdot\text{m}^{-2}\cdot\text{day}^{-1}$) | OP ($\text{cm}^3\cdot\text{mil}\cdot\text{m}^{-2}\cdot\text{day}^{-1}$) | WVTR ($\text{g}\cdot\text{m}^{-2}\cdot\text{day}^{-1}$) | OTR ($\text{cm}^3\cdot\text{m}^{-2}\cdot\text{day}^{-1}$) |
|-----------------------|---|---|---|---|
| 2,7-CPPI ¹ | 0.3 ± 0.02 | 0.5 ± 0.03 | 0.1 ± 0.01 | 0.2 ± 0.01 |
| M-2,7-CPPI | 30.3 ± 0.6 | 35.8 ± 0.6 | 10.2 ± 0.2 | 12.1 ± 0.2 |

¹ The barrier properties values are obtained from Ref. [26].

3.5. Aggregation Structure Analysis

The aggregation structure of PIs was investigated with WAXD, as shown in Figure 3. The *meta*-isomer M-2,7-CPPI showed a diffraction peak at 15.10° with *d*-spacing of 5.86 \AA , while in *para*-based 2,7-CPPI, the diffraction peak was shifted to 21.91° with *d*-spacing low to 4.05 \AA (Table 3), implying the loose molecular packing of M-2,7-CPPI. The density of M-2,7-CPPI was smaller than that of 2,7-CPPI (Table 3). Additionally, the chain stacking was determined by radial distribution functions (RDFs). The interchain RDFs based on all the C atoms in the benzene ring and all N atoms in the imide ring are analyzed and displayed in Figure S12a,b, respectively. M-2,7-CPPI demonstrated a lower $g(r)$ value than 2,7-CPPI in Figure S12a. The chain packing difference between the two isomeric polyimides may be a consequence of chain morphology.

**Figure 3.** WAXD curve of M-2,7-CPPI and 2,7-CPPI films.**Table 3.** Physical properties of the M-2,7-CPPI and 2,7-CPPI.

| PI | Density ($\text{g}\cdot\text{cm}^{-3}$) | 2θ ($^\circ$) | <i>d</i> -Spacing (\AA) | R_g (\AA) | N ¹ (H-Bonds) | CED ($\text{J}\cdot\text{cm}^{-3}$) |
|------------|---|------------------------|------------------------------------|------------------------|--------------------------|---------------------------------------|
| 2,7-CPPI | 1.57 | 21.91 | 4.05 | 54.3 | 49 | 570 |
| M-2,7-CPPI | 1.56 | 15.10 | 5.86 | 47.5 | 38 | 456 |

¹ The number of hydrogen bonds in the simulation cells.

Figure 4 illustrates the polymer chain conformation of M-2,7-CPPI and 2,7-CPPI with 25 repeat units under the lowest energy. The *meta*-isomer M-2,7-CPPI showed bent and distorted chain structure, whereas that of 2,7-CPPI was linear and regular. In addition, the radius of gyration (R_g) was studied for the two isomeric polyimides. The R_g as a function of time for the equilibrated M-2,7-CPPI and 2,7-CPPI are illustrated in Figure S13. The average R_g values are given in Table 3. 2,7-CPPI showed a larger R_g than M-2,7-CPPI, indicating its more stretched chain structure [34].

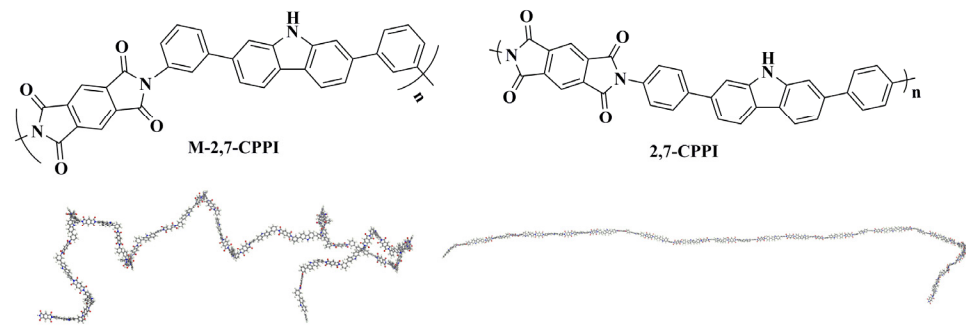


Figure 4. The polymer chain conformations of M-2,7-CPPI and 2,7-CPPI under the lowest energy.

3.6. Hydrogen Bonds Analysis

Intermolecular forces also affect chain stacking. For M-2,7-CPPI and 2,7-CPPI, hydrogen bonds can be formed between O=C– and –NH–. The radial distribution functions ($g_{AB}(r)$) of O atoms in O=C– and H atoms in –HN– were determined for M-2,7-CPPI and 2,7-CPPI to study the hydrogen bonds. The result is given in Figure 5. Hydrogen bond forces are considered to have the distances between atoms of 2.6–3.1 Å [35]. In Figure 5, peaks were observed in the range of 2.6–3.1 Å for the two PIs, proving that hydrogen bonds were formed. Obviously, 2,7-CPPI displayed a larger $g(r)$ value than M-2,7-CPPI in that range, implying there are more hydrogen bonds in the 2,7-CPPI matrix. Figure 6 illustrates the hydrogen bonds generated in the M-2,7-CPPI cell, verifying the presence of hydrogen bonds between O=C– and –NH–. Statistical analysis indicated that 38 and 49 hydrogen bonds were generated in the M-2,7-CPPI and 2,7-CPPI cells, respectively (Table 3). When the linkage was changed from *para* to *meta*, the regularity of polymer chains in M-2,7-CPPI was decreased, and the compact chain stacking was hampered. The less ordered and packed structure of M-2,7-CPPI hindered the formation of hydrogen bonds, leading to a decreased number of hydrogen bonds. This also can be revealed from the cohesive energy density (CED) results in Table 3. The CED of 2,7-CPPI was 570 J/cm³, which decreased to 456 J/cm³ for M-2,7-CPPI. The distorted chain structure and weak hydrogen bonding gave rise to the loose chain packing of M-2,7-CPPI.

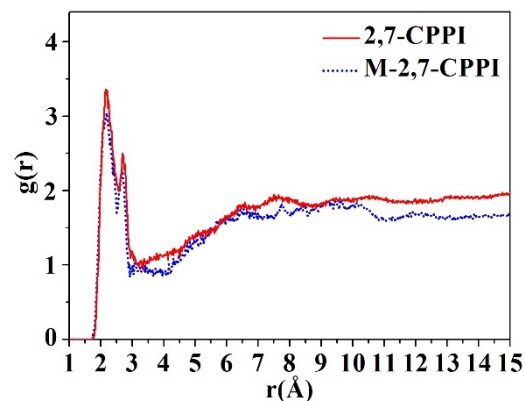


Figure 5. The RDFs of the hydrogen atoms of –HN– in carbazole and oxygen atoms of O=C– in imide rings for M-2,7-CPPI and 2,7-CPPI.

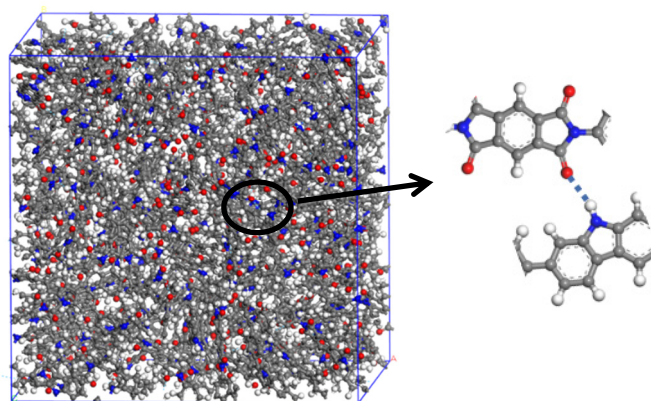


Figure 6. H-bonds between —HN— and O=C— in simulation cell of M-2,7-CPPI.

3.7. Free Volumes Analysis

3.7.1. Positron Annihilation Test

The molecular chain morphology and aggregation structure have a substantial effect on the free volumes of PIs and thereby the barrier performances [36,37]. Positron annihilation lifetime spectroscopy (PALS) was utilized to analyze the free volumes of PIs. The positron lifetime plots and data are shown in Figure 7 and Table 4. Based on the second lifetime component (τ_2) and its intensity (I_2), the mean radius (R) and size (V_{f2}) of free volume and relative fractional free volume (FFV) were determined according to our previous study [26]. The *para*-isomer 2,7-CPPI showed R and FFV of 2.14 Å and 6.82%, whereas, for *meta*-based M-2,7-CPPI, those were increased to 2.26 Å and 7.46%.

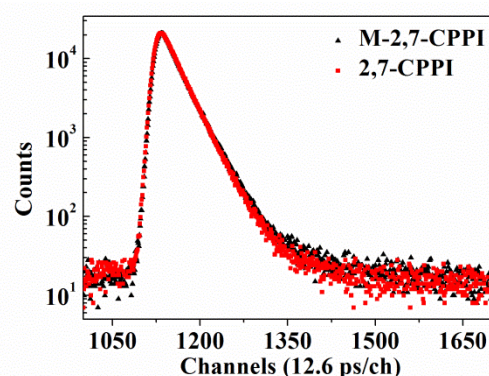


Figure 7. Positron lifetime spectra measured for the M-2,7-CPPI and 2,7-CPPI films.

Table 4. The analyzed data for the positron lifetime in the M-2,7-CPPI and 2,7-CPPI films.

| PI | τ_1 (ns) | I_1 (%) | τ_2 (ns) | I_2 (%) | R (Å) | V_{f2} (Å ³) | FFV^1 (%) | FFV^2 (O ₂ ,%) | FFV^2 (H ₂ O,%) | FFV^{02} (%) |
|-----------------------|------------------|--------------|------------------|--------------|------------|-------------------------------|----------------|--------------------------------|---------------------------------|-------------------|
| 2,7-CPPI ³ | 0.17 | 7.4 | 0.34 | 92.4 | 2.14 | 41.03 | 6.82 | 6.29 | 11.51 | 35.33 |
| M-2,7-CPPI | 0.16 | 12.6 | 0.35 | 85.7 | 2.26 | 48.33 | 7.46 | 7.05 | 12.32 | 37.90 |

¹ FFV determined by PALS. ² Free volume parameters calculated by simulations, FFV (O₂), FFV (H₂O) and FFV^0 based on probe radii of 1.73 Å, 1.325 Å and 0 Å, respectively. ³ The values are obtained from Ref. [26].

3.7.2. Molecular Simulations

Free volume features, including size distribution and connectivity, were considered as key parameters determining gas transport performance [38,39]. Molecular simulations were conducted to study the free volume. The distributions of void size were shown in Figure 8a. Compared with *para*-isomer 2,7-CPPI, *meta*-based M-2,7-CPPI had a greater number of holes with a radius larger than 0.8 Å, but fewer holes with a radius smaller than 0.8 Å. The kinetic

radii of H₂O and O₂ are larger than 0.8 Å (O₂: 1.73 Å, H₂O: 1.325 Å). This suggested that M-2,7-CPPI had more cavities for H₂O and O₂ permeation in comparison with 2,7-CPPI, which led to high gas permeability and therefore decreased barrier performances of M-2,7-CPPI.

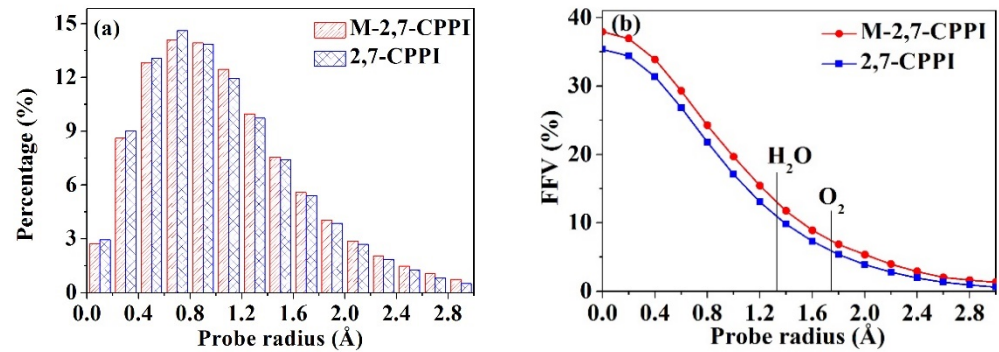


Figure 8. Distributions of void radius (a) and fractional free volume (b) as a function of probe radius in M-2,7-CPPI and 2,7-CPPI. The kinetic radii of O₂ and H₂O are indicated by vertical lines.

The relationships between probe radius and *FFV* of the two PIs are studied and shown in Figure 8b. With the increase of probe radius, the *FFV* of the two polyimides decreased. The *meta*-based M-2,7-CPPI exhibited larger *FFV* than 2,7-CPPI in the whole radius range. The total fractional free volume (*FFV*⁰) was simulated using a probe radius of 0 Å. The *FFV* (O₂) and *FFV* (H₂O) were also calculated using the kinetic radii of O₂ and H₂O as probe radii. Table 4 lists the *FFV*⁰, *FFV* (O₂) and *FFV* (H₂O) values. The *meta*-based M-2,7-CPPI showed higher *FFV* values than 2,7-CPPI, in agreement with the PALS analysis. The accessible volume morphologies of H₂O and O₂ in the two PIs are presented in Figure 9. The *para*-isomer 2,7-CPPI possessed smaller and disconnected holes, while those in *meta*-based M-2,7-CPPI were bigger and well-connected. Changing the linkage from *para* to *meta* reduced the molecular chain order, which hindered the tight chain packing and weakened the intermolecular hydrogen bonding. Consequently, the number and size of free volumes increased, thus bringing about high gas permeability and thereby decreased barrier performances of M-2,7-CPPI.

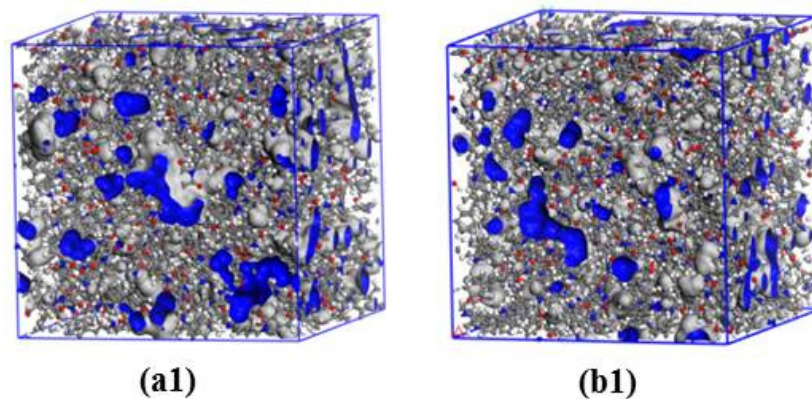


Figure 9. Cont.

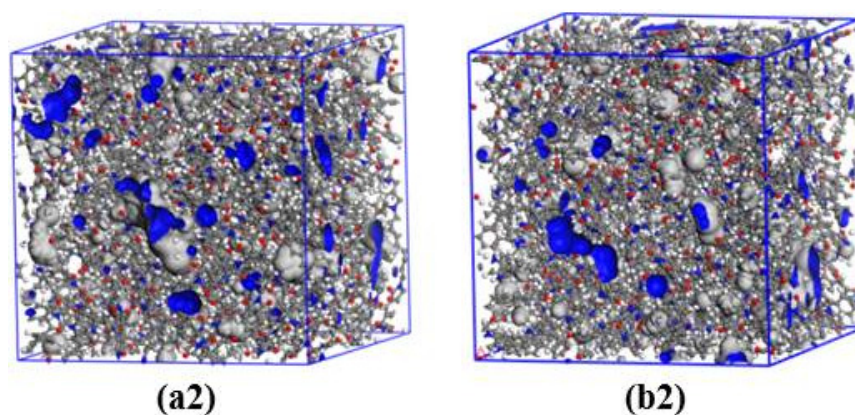


Figure 9. Three-dimensional representation of H₂O and O₂ accessible volume for (a1,a2) M-2,7-CPPI and (b1,b2) 2,7-CPPI. (grey: Van der Waals surface; blue: Connolly surface; (a1,b1): probe radius of 1.325 Å; (a2,b2): probe radius of 1.73 Å).

3.8. Gas Transport Behavior

From the perspectives of gas diffusion and solubility, gas transport behavior is investigated to understand the barrier performance difference between the two isomeric polyimides.

3.8.1. Gas Diffusivity

The diffusivity behaviors, including trajectory and displacement of O₂ and H₂O in the PI matrices, were studied and shown in Figure 10 and Figure S14, respectively. Oxygen and water molecules had two motion statuses in the PI matrix. One was the oscillation in the voids, and the other was occasional jumps from one void to an adjacent void [40]. As shown in Figure 10 and Figure S14, the movement distance and frequency of oxygen and water in *para*-isomer 2,7-CPPI were lower, whereas those in *meta*-based M-2,7-CPPI were larger, indicating that oxygen and water had higher mobility in the M-2,7-CPPI matrix.

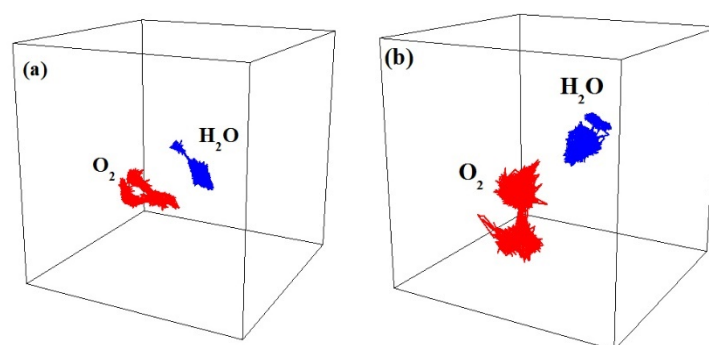


Figure 10. The representative trajectories of O₂ and H₂O in (a) 2,7-CPPI and (b) M-2,7-CPPI.

The MSD vs. time plots of H₂O and O₂ in the two polyimides are presented in Figure 11. According to Einstein's equation, the diffusion coefficients (*D*) of O₂ and H₂O were determined from normal diffusion interval, in which the plot slope was unity. The *D* values are shown in Table 5. The *meta*-based M-2,7-CPPI displayed larger *D* values of H₂O and O₂ compared with those of 2,7-CPPI. Changing the linkage from *para* to *meta* disrupted chain packing and weakened intermolecular forces, thus leading to increased free volume. As a result, the diffusion coefficients of H₂O and O₂ were enhanced in M-2,7-CPPI. Additionally, it can be found that in a fixed PI matrix, the *D* of O₂ was larger than that of H₂O, even though the kinetic radius of O₂ was bigger. This was mainly owing to the high interaction between the polar water molecule and the PI, impeding H₂O diffusion [41].

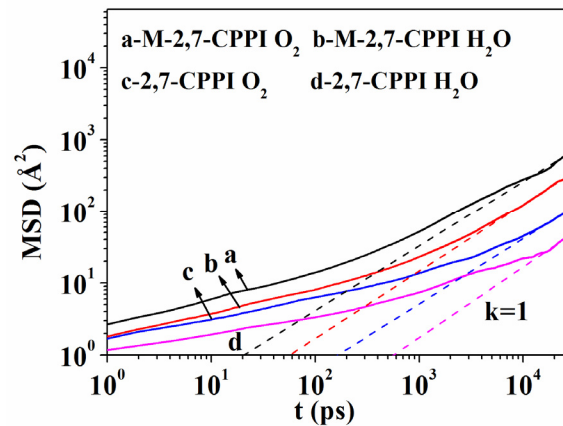


Figure 11. MSD of O₂ and H₂O in M-2,7-CPPI and 2,7-CPPI as a function of time.

Table 5. Simulated diffusion coefficients, solubility coefficients and permeability for O₂ and H₂O in M-2,7-CPPI and 2,7-CPPI.

| PIs | D ¹ | | S ² | | P ³ | |
|------------|------------------|----------------|------------------|----------------|------------------|----------------|
| | H ₂ O | O ₂ | H ₂ O | O ₂ | H ₂ O | O ₂ |
| 2,7-CPPI | 3.24 | 6.55 | 0.64 | 0.013 | 2.07 | 0.09 |
| M-2,7-CPPI | 7.84 | 14.20 | 2.39 | 0.044 | 18.74 | 0.62 |

¹ Units of (10⁻⁸cm²/s). ² Units of (cm³(STP) cm⁻³·cmHg⁻¹). ³ Units of (10⁻⁸cm²·cm³(STP)·s⁻¹·cm⁻³·cmHg⁻¹).

3.8.2. Gas Solubility

For a better understanding of gas sorption behaviors, the gas sorption isotherms of H₂O and O₂ were analyzed and exhibited in Figure 12. The sorption isotherms of H₂O and O₂ in the two PIs can be elucidated by a typical dual-mode sorption model [42]. When the pressure was low, the Langmuir's sorption dominated, which occurred in the micro-voids. At high pressures, Henry mode sorption took place in free volume among the chains. The obtained solubility coefficients (S) in M-2,7-CPPI and 2,7-CPPI are listed in Table 5. The *meta*-based M-2,7-CPPI presented higher S values of H₂O and O₂ than *para*-based 2,7-CPPI. In addition, the sorption sites of H₂O and O₂ in the two PIs are displayed in Figure 13. M-2,7-CPPI had larger sorption loading of H₂O and O₂ than 2,7-CPPI. As discussed above, *meta*-based M-2,7-CPPI possessed a larger number and size of free volumes, providing more sites for gas sorption. This was the main reason for the higher S value in M-2,7-CPPI. It is worth mentioning that the S of H₂O was higher than that of O₂ in a fixed PI. This was mostly ascribed to the high affinity between PI and H₂O and the smaller size and high critical temperature of H₂O [43].

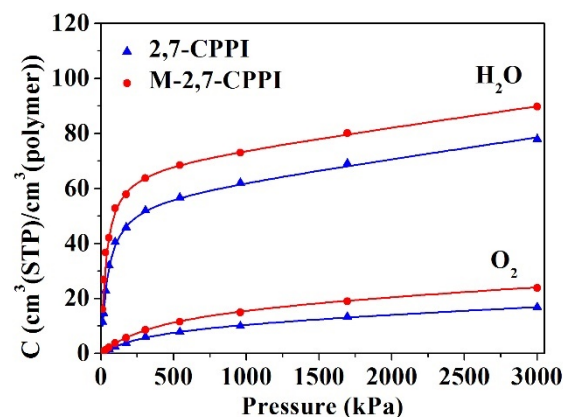


Figure 12. The adsorption isotherms of O₂ and H₂O in M-2,7-CPPI and 2,7-CPPI.

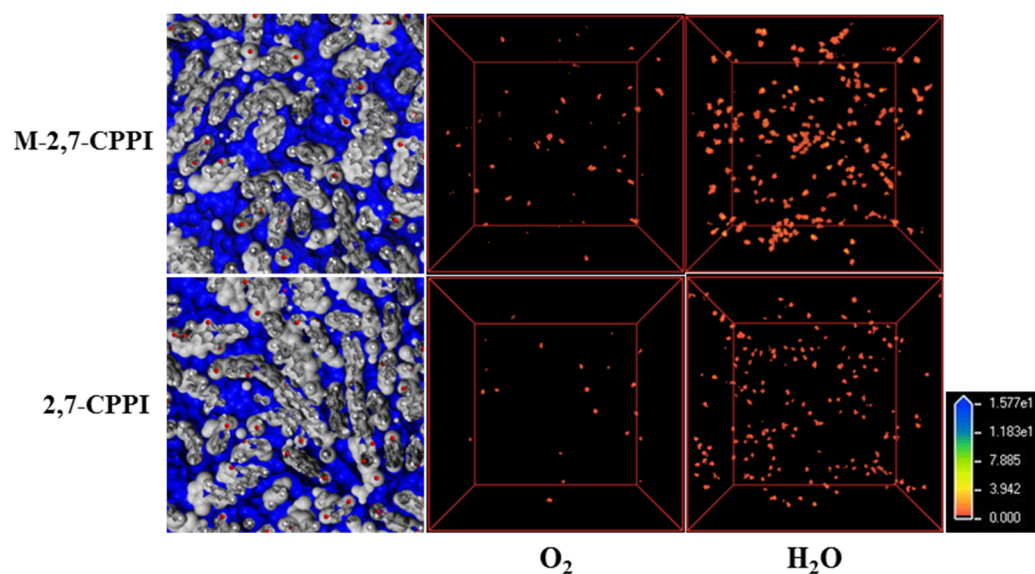


Figure 13. Sorption sites of O₂ and H₂O in M-2,7-CPPI and 2,7-CPPI. (Red, yellow, and blue stand for low, medium, and high adsorption amounts, respectively.).

3.8.3. Gas Permeability

The permeability coefficient (P) was calculated with the equation $P = D \times S$ as elucidated by the solution-diffusion mechanism [44] and is shown in Table 5. The simulated P of O₂ and H₂O in the two isomeric polyimides displayed the same variation trend with the experimental values, proving the viability of molecular simulation on gas permeability. Altering the linkage from *para* to *meta* impeded the dense chain stacking and thus increased free volumes, promoting the gases diffusivity and solubility. Consequently, the *meta*-based isomer M-2,7-CPPI showed increased gas permeability and therefore reduced barrier properties.

4. Conclusions

A diamine (M-2,7-CPDA) bearing carbazole moiety was synthesized by a two-step method. This diamine is an isomer of our previously reported diamine 2,7-CPDA, in which the substituted position of amino is altered from *para* to *meta*. Both diamines were polymerized with PMDA to obtain two isomeric polyimides (M-2,7-CPPI and 2,7-CPPI). The two isomeric PIs showed comparable thermal stability. *Meta*-linked M-2,7-CPPI had lower mechanical properties and higher CTE than *para*-linked 2,7-CPPI. Molecular simulation, PALS and WAXD were employed to explore the effect of molecular isomerism on barrier performances of polyimides. Compared with *para*-linked 2,7-CPPI, *meta*-linked M-2,7-CPPI displayed loose chain stacking caused by the less ordered chain structure and weaker hydrogen bonding, which led to higher *FFV* of M-2,7-CPPI. The higher free volumes benefited the gases diffusivity and solubility in M-2,7-CPPI matrix. Consequently, the *meta*-linked M-2,7-CPPI displayed a lower gas barrier than its *para*-linked analog. This research provides inspiration for the design of high-performance barrier polymers.

Supplementary Materials: The following are available online at <https://www.mdpi.com/article/10.3390/polym13111749/s1>. Materials and instrumentation. Details of molecular simulation. ¹H NMR, ¹³C NMR spectra and mass spectrum of M-2,7-CPDN. Mass spectrum of M-2,7-CPDA. FT-IR spectra of M-2,7-CPDN, M-2,7-CPDA and M-2,7-CPPI. TGA, DSC, DMA and TMA curves of M-2,7-CPPI film. The $g(r)$, R_g and displacement of O₂ and H₂O for M-2,7-CPPI and 2,7-CPPI.

Author Contributions: Y.L. and J.T.: writing—original draft, writing—review and editing, conceptualization, project administration, funding acquisition; F.X., J.H., W.S.: project administration, resources, investigation, methodology; C.C., L.J.: formal analysis, investigation, methodology; H.Z.: Writing—review and editing, supervision, project administration. All authors have read and agreed to the published version of the manuscript.

Funding: This research was funded by NSAF (U1930203), National Natural Science Foundation of China (No. 51973055), the Natural Science Foundation of Hunan Province (No. 2019JJ40071), the Key R & D Project of Hunan Province (No. 2018GK2063) and the Student Innovation and Entrepreneurship Training Program of China (No. 201911535005).

Institutional Review Board Statement: Not applicable.

Informed Consent Statement: Not applicable.

Data Availability Statement: The data presented in this study are available on request from the corresponding author.

Acknowledgments: We would like to thank Zhiqian Chen from Hubei Nuclear Solid Physics Key Laboratory, Department of Physics, Wuhan University for their help in the measurement of the polymer free volume.

Conflicts of Interest: The authors declare no competing financial interest.

References

1. Windrich, F.; Kappert, E.J.; Malanin, M.; Eichhorn, K.-J.; Häußler, L.; Benes, N.E.; Voit, B. In-situ imidization analysis in microscale thin films of an ester-type photosensitive polyimide for microelectronic packaging applications. *Eur. Polym. J.* **2016**, *84*, 279–291. [[CrossRef](#)]
2. Pakhuruddin, M.Z.; Ibrahim, K.; Aziz, A.A. Properties of polyimide substrate for applications in flexible solar cells. *J. Optoelectron. Adv. Mater.* **2013**, *7*, 377–380.
3. Jagadish, R.S.; Raj, B.; Asha, M.R. Blending of low-density polyethylene with vanillin for improved barrier and aroma-releasing properties in food packaging. *J. Appl. Polym. Sci.* **2009**, *113*, 3732–3741. [[CrossRef](#)]
4. Liaw, D.-J.; Wang, K.-L.; Huang, Y.-C.; Lee, K.-R.; Lai, J.-Y.; Ha, C.-S. Advanced polyimide materials: Syntheses, physical properties and applications. *Prog. Polym. Sci.* **2012**, *37*, 907–974. [[CrossRef](#)]
5. Yi, C.; Li, W.; Shi, S.; He, K.; Ma, P.; Chen, M.; Yang, C. High-temperature-resistant and colorless polyimide: Preparations, properties, and applications. *Sol. Energy* **2020**, *195*, 340–354. [[CrossRef](#)]
6. Choi, M.-C.; Kim, Y.; Ha, C.-S. Polymers for flexible displays: From material selection to device applications. *Prog. Polym. Sci.* **2008**, *33*, 581–630. [[CrossRef](#)]
7. Tiwari, A.N.; Romeo, A.; Baetzner, D.; Zogg, H. Flexible CdTe solar cells on polymer films. *Prog. Photovolt.* **2001**, *9*, 211–215. [[CrossRef](#)]
8. Salleo, A.; Street, R.A. Light-induced bias stress reversal in polyfluorene thin-film transistors. *J. Appl. Phys.* **2003**, *94*, 471–479. [[CrossRef](#)]
9. Street, R.A. Thin-film transistors. *Adv. Mater.* **2009**, *21*, 2007–2022. [[CrossRef](#)]
10. Zekriar dehani, S.; Jabarin, S.A.; Gidley, D.R.; Coleman, M.R. Effect of chain dynamics, crystallinity, and free volume on the barrier properties of poly(ethylene terephthalate) biaxially oriented films. *Macromolecules* **2017**, *50*, 2845–2855. [[CrossRef](#)]
11. Xu, H.; Luo, D.; Li, M.; Xu, M.; Zou, J.; Tao, H.; Lin-Feng, L.; Wang, L.; Peng, J.; Cao, Y. A flexible AMOLED display on the PEN substrate driven by oxide thin-film transistors using anodized aluminium oxide as dielectric. *J. Mater. Chem. C* **2014**, *2*, 1255–1259. [[CrossRef](#)]
12. Hu, Y.S.; Mehta, S.; Schiraldi, D.A.; Hiltner, A.; Baer, E. Effect of water sorption on oxygen-barrier properties of aromatic polyamides. *J. Polym. Sci. Part B Polym. Phys* **2005**, *43*, 1365–1381. [[CrossRef](#)]
13. Hwang, T.; Pu, L.; Kim, S.W.; Oh, Y.-S.; Nam, J.-D. Synthesis and barrier properties of poly(vinylidene chloride-co-acrylonitrile)/SiO₂ hybrid composites by sol-gel process. *J. Membr. Sci.* **2009**, *345*, 90–96. [[CrossRef](#)]
14. Maes, C.; Luyten, W.; Herremans, G.; Peeters, R.; Carleer, R.; Buntinx, M. Recent updates on the barrier properties of ethylene vinyl alcohol copolymer (EVOH): A review. *Polym. Rev.* **2018**, *58*, 209–246. [[CrossRef](#)]
15. Liu, Y.; Qian, C.; Qu, L.; Wu, Y.; Zhang, Y.; Wu, X.; Zou, B.; Chen, W.; Chen, Z.; Chi, Z.; et al. A bulk dielectric polymer film with intrinsic ultralow dielectric constant and outstanding comprehensive properties. *Chem. Mater.* **2015**, *27*, 6543–6549. [[CrossRef](#)]
16. Li, T.-L.; Hsu, S.L.-C. Preparation and properties of a high temperature, flexible and colorless ITO coated polyimide substrate. *Eur. Polym. J.* **2007**, *43*, 3368–3373. [[CrossRef](#)]
17. Sykes, G.F.; Clair, A.K.S. The effect of molecular structure on the gas transmission rates of aromatic polyimides. *J. Appl. Polym. Sci.* **1986**, *32*, 3725–3735. [[CrossRef](#)]
18. Coleman, M.; Koros, W. The transport properties of polyimide isomers containing hexafluoroisopropylidene in the diamine residue. *J. Polym. Sci. Part B Polym. Phys.* **1994**, *32*, 1915–1926. [[CrossRef](#)]
19. Madzarevic, Z.P.; Shahid, S.; Nijmeijer, K.; Dingemans, T.J. The role of ortho-, meta- and para-substitutions in the main-chain structure of poly(etherimide)s and the effects on CO₂/CH₄ gas separation performance. *Sep. Purif. Technol.* **2019**, *210*, 242–250. [[CrossRef](#)]
20. Coleman, M.; Koros, W. Isomeric polyimides based on fluorinated dianhydrides and diamines for gas separation applications. *J. Membr. Sci.* **1990**, *50*, 285–297. [[CrossRef](#)]

21. Wang, Y.; Tao, L.; Wang, T.; Wang, Q. Influence of monomer conformation on the mechanical and tribological properties of thermosetting polyimides. *RSC Adv.* **2015**, *5*, 101533–101543. [[CrossRef](#)]
22. Comesaña-Gándara, B.; Calle, M.; Jo, H.J.; Hernández, A.; de la Campa, J.G.; de Abajo, J.; Lozano, A.E.; Lee, Y.M. Thermally rearranged polybenzoxazoles membranes with biphenyl moieties: Monomer isomeric effect. *J. Membr. Sci.* **2014**, *450*, 369–379. [[CrossRef](#)]
23. Song, G.; Zhang, Y.; Wang, D.; Chen, C.; Zhou, H.; Zhao, X.; Dang, G. Intermolecular interactions of polyimides containing benzimidazole and benzoxazole moieties. *Polymer* **2013**, *54*, 2335–2340. [[CrossRef](#)]
24. Pei, X.; Chen, G.; Hou, Y.; Fang, X. Comparative study on polyimides derived from isomeric diphenylsulfonetetracarboxylic dianhydrides. *High Perform. Polym.* **2012**, *25*, 312–323. [[CrossRef](#)]
25. Zhang, M.; Wang, Z.; Gao, L.; Ding, M. Polyimides from isomeric diphenylthioether dianhydrides. *J. Polym. Sci. Part A Polym. Chem.* **2006**, *44*, 959–967. [[CrossRef](#)]
26. Liu, Y.; Huang, J.; Tan, J.; Zeng, Y.; Liu, J.; Zhang, H.; Pei, Y.; Xiang, X.; Liu, Y. Intrinsic high-barrier polyimide with low free volume derived from a novel diamine monomer containing rigid planar moiety. *Polymer* **2017**, *114*, 289–297. [[CrossRef](#)]
27. Chang, K.-S.; Tung, C.-C.; Wang, K.-S.; Tung, K.-L. Free volume analysis and gas transport mechanisms of aromatic polyimide membranes: A molecular simulation study. *J. Phys. Chem. B* **2009**, *113*, 9821–9830. [[CrossRef](#)]
28. Okada, T.; Ishige, R.; Ando, S. Effects of chain packing and structural isomerism on the anisotropic linear and volumetric thermal expansion behaviors of polyimide films. *Polymer* **2018**, *146*, 386–395. [[CrossRef](#)]
29. Ando, S.; Sekiguchi, K.; Mizoroki, M.; Okada, T.; Ishige, R. Anisotropic linear and volumetric thermal-expansion behaviors of self-standing polyimide films analyzed by thermomechanical analysis (TMA) and optical interferometry. *Macromol. Chem. Phys.* **2018**, *219*, 1700354. [[CrossRef](#)]
30. Kochi, M.; Chen, C.; Yokota, R.; Hasegawa, M.; Hergenrother, P. Isomeric biphenyl polyimides. (II) glass transitions and secondary relaxation processes. *High Perform. Polym.* **2016**, *17*, 335–347. [[CrossRef](#)]
31. Ishii, J.; Takata, A.; Oami, Y.; Yokota, R.; Vladimirov, L.; Hasegawa, M. Spontaneous molecular orientation of polyimides induced by thermal imidization (6). Mechanism of negative in-plane CTE generation in non-stretched polyimide films. *Eur. Polym. J.* **2010**, *46*, 681–693. [[CrossRef](#)]
32. Inagaki, N.; Cech, V.; Narushima, K.; Takechi, Y. Oxygen and water vapor gas barrier poly(ethylene naphthalate) films by deposition of SiO_x plasma polymers from mixture of tetramethoxysilane and oxygen. *J. Appl. Polym. Sci.* **2007**, *104*, 915–925. [[CrossRef](#)]
33. Gargalaka, J.; Couto, R.A.A.; Constantino, V.R.L.; Toma, H.E.; Araki, K. Influence of the relative amounts of crystalline and amorphous phases on the mechanical properties of polyamide-6 nanocomposites. *J. Appl. Polym. Sci.* **2012**, *125*, 3239–3249. [[CrossRef](#)]
34. Park, C.H.; Tocci, E.; Lee, Y.M.; Drioli, E. Thermal treatment effect on the structure and property change between hydroxy-containing polyimides (HPIs) and thermally rearranged polybenzoxazole (TR-PBO). *J. Phys. Chem. B* **2012**, *116*, 12864–12877. [[CrossRef](#)] [[PubMed](#)]
35. Mattozzi, A.; Hedenqvist, M.S.; Gedde, U.W. Diffusivity of n-hexane in poly(ethylenestat-octene)s assessed by molecular dynamics simulation. *Polymer* **2007**, *48*, 5174–5180. [[CrossRef](#)]
36. Miyata, S.; Sato, S.; Nagai, K.; Nakagawa, T.; Kudo, K. Relationship between gas transport properties and fractional free volume determined from dielectric constant in polyimide films containing the hexafluoroisopropylidene group. *J. Appl. Polym. Sci.* **2008**, *107*, 3933–3944. [[CrossRef](#)]
37. Low, B.T.; Chung, T.S.; Chen, H.; Jean, Y.-C.; Pramoda, K.P. Tuning the free volume cavities of polyimide membranes via the construction of pseudo-interpenetrating networks for enhanced gas separation performance. *Macromolecules* **2009**, *42*, 7042–7054. [[CrossRef](#)]
38. Belov, N.A.; Zharov, A.A.; Shashkin, A.V.; Shaikh, M.Q.; Raetzke, K.; Yampolskii, Y.P. Gas transport and free volume in hexafluoropropylene polymers. *J. Membr. Sci.* **2011**, *383*, 70–77. [[CrossRef](#)]
39. Hu, C.-C.; Chang, C.-S.; Ruaan, R.-C.; Lai, J.-Y. Effect of free volume and sorption on membrane gas transport. *J. Membr. Sci.* **2003**, *226*, 51–61. [[CrossRef](#)]
40. Neyertz, S.; Brown, D.; Pandiyan, S.; van der Vegt, N.F.A. Carbon dioxide diffusion and plasticization in fluorinated polyimides. *Macromolecules* **2010**, *43*, 7813–7827. [[CrossRef](#)]
41. Musto, P.; Ragosta, G.; Mensitieri, G.; Lavorgna, M. On the molecular mechanism of H₂O diffusion into polyimides: A vibrational spectroscopy investigation. *Macromolecules* **2007**, *40*, 9614–9627. [[CrossRef](#)]
42. Zhang, Y.; Lee, W.H.; Seong, J.G.; Bae, J.Y.; Zhuang, Y.; Feng, S.; Wan, Y.; Lee, Y.M. Alicyclic segments upgrade hydrogen separation performance of intrinsically microporous polyimide membranes. *J. Membr. Sci.* **2020**, *611*, 118363. [[CrossRef](#)]
43. Zhang, K.; Yu, Q.; Zhu, L.; Liu, S.; Chi, Z.; Chen, X.; Zhang, Y.; Xu, J. The preparations and water vapor barrier properties of polyimide films containing amide moieties. *Polymers* **2017**, *9*, 677. [[CrossRef](#)] [[PubMed](#)]
44. Wijmans, J.G.; Baker, R. The solution-diffusion model: A review. *J. Membr. Sci.* **1995**, *107*, 1–21. [[CrossRef](#)]